Gamma-ray Constraints on Dark Matter Annihilation into Charged Particles

Nicole F. Bell[1] and Thomas D. Jacques[1]

[1]*School of Physics, The University of Melbourne, Victoria 3010, Australia*

(Dated: February 5, 2009)

Dark matter annihilation into charged particles is necessarily accompanied by gamma rays, produced via radiative corrections. Internal bremsstrahlung from the final state particles can produce hard gamma rays up to the dark matter mass, with an approximately model-independent spectrum. Focusing on annihilation into electrons, we compute robust upper bounds on the dark matter self annihilation cross section $\langle\sigma_A v\rangle_{e^+e^-}$ using gamma-ray data from the Milky Way spanning a wide range of energies, $\sim 10^{-3} - 10^4$ GeV. We also compute corresponding bounds for the other charged leptons. We make conservative assumptions about the astrophysical inputs, and demonstrate how our derived bounds would be strengthened if stronger assumptions about these inputs are adopted. The fraction of hard gamma rays near the end point accompanying annihilation to e^+e^- is only a factor of $\lesssim 10^2$ lower than for annihilation directly to monoenergetic gamma rays. The bound on $\langle\sigma_A v\rangle_{e^+e^-}$ is thus weaker than that for $\langle\sigma_A v\rangle_{\gamma\gamma}$ by this same factor. The upper bounds on the annihilation cross sections to charged leptons are compared with an upper bound on the *total* annihilation cross section defined by neutrinos.

PACS numbers: 95.35.+d, 95.85.Pw, 98.70.Vc, 98.62.Gq

I. INTRODUCTION

A wealth of observational evidence attests to the existence of dark matter (DM) (see, e.g., Refs. [1–3] for reviews). However, despite the fact that DM accounts for a large fraction of the total energy density of the Universe, it has evaded direct detection and its particle properties remain unknown.

If dark matter is a thermal relic, it should have a small, but non-negligible, self annihilation cross section. This allows a means of indirect detection of DM, as annihilations in the Universe today may generate an observable flux of products. For thermal relic DM, a total annihilation cross section of $\langle\sigma_A v\rangle \sim 3 \times 10^{-26}\mathrm{cm}^3\ \mathrm{s}^{-1}$ is needed in order to obtain the observed relic abundance of $\Omega_{\rm DM} \simeq 0.3$. (We shall work with the quantity $\langle\sigma_A v\rangle$, which is the product of the annihilation cross section and relative velocity, averaged over the dark matter velocity distribution. In the Milky Way, $v_{\rm rms} \sim 10^{-3}c$.) If DM is not a thermal relic, e.g., Refs. [4–6], even larger annihilation cross sections are possible. There have also been a number of recent proposals in which $\langle\sigma_A v\rangle$ is enhanced at low velocity [7–9, 14–20] (i.e., in galactic halos) while still satisfying the thermal relic constraints. (Note that these scenarios are subject to constraints arising from annihilations in the first collapsed structures [21].)

While the total cross section may be related to the relic abundance, the branching ratios to any particular final states are model-dependent. If we assume the DM is the lightest new particle beyond those in the standard model (SM), then the branching ratio to SM final states must be 100%. Annihilations must then produce fluxes of detectable particles emanating from regions of DM concentration, with signals such as gamma rays, microwaves, neutrinos, and positrons being of particular interest. There exist general constraints on the total annihilation cross-section, based upon unitarity [22, 23] and the requirement that annihilations not significantly alter halo density profiles [6]. A strong bound is placed on the total annihilation cross section by assuming that the branching ratio to neutrinos, the least detectable final state, is 100% [24, 25].

We focus here on the process $\chi\chi \to e^+e^-$ in which DM annihilates to an electron-positron pair, though we shall also report results for the other charged leptons. Although the branching ratio to this particular final state is model-dependent, it is a significant channel in a wide range of models. For example, while annihilation to fermions is helicity suppressed in supersymmetric models, Kaluza-Klein DM features large (unsuppressed) annihilation rates to leptons [10–12], as does the Dirac DM model of Ref. [13]. Numerous authors have recently proposed models in which annihilation to charged leptons is significantly enhanced [14–20], making upper limits on the cross section to these annihilation products particularly interesting. In addition, various other SM final states, such as W^+W^- and ZZ, produce l^+l^- via their decays and hence a flux of charged leptons is of generic interest in a large variety of DM models.

Several techniques may be used to constrain the production of e^+e^- within galactic halos, all of which rely on the fact the charged particles inevitably produce photons. Signals considered include gamma rays, x-rays, microwaves and radio waves. Photons are produced by the various energy loss processes that charged particles undergo in a galactic halo, examples of which include synchrotron radiation due to the propagation of $e^\pm$ in galactic magnetic fields, and inverse Compton scattering of electrons from interstellar radiation fields, e.g., [26–35]. The drawback of these techniques is a significant dependence on astrophysical inputs, some of which are poorly known. Uncertainties in magnetic field strengths, radiation backgrounds, and electron diffusion scales all enter the calculations in an involved fashion.

Charged particles also produce photons via electromagnetic radiative corrections [36–44]. The lowest order dark matter annihilation process $\chi\chi \to e^+e^-$ is necessarily accompanied by the radiative correction $\chi\chi \to e^+e^-\gamma$. This is an *internal bremsstrahlung* (IB) process, meaning that the photon arises at the Feynman diagram level and is not due to interaction of charged particles in a medium. Importantly, for a given annihilation cross section, $\langle\sigma_A v\rangle_{e^+e^-}$, the accompanying flux of IB photons can be determined without knowledge of the new underlying particle physics which mediates the DM annihilation. Moreover, IB suffers none the drawbacks of the competing inverse Compton and synchrotron techniques outlined above. While inverse Compton and synchrotron fluxes are dependent on conditions of the astrophysical environment, the IB flux is always present and its normalization and spectrum are predetermined.

In this paper we use IB emission to derive robust upper limits on the dark matter annihilation cross section to electron-positron pairs $\langle\sigma_A v\rangle_{e^+e^-}$ over a wide DM mass range spanning $\sim 10^{-3} - 10^4$ GeV. We calculate DM annihilation fluxes produced in the galactic halo, and compare with the gamma-ray backgrounds reported by COMPTEL, EGRET and H.E.S.S. We also look at data for the M31 (Andromeda) galaxy, to fill a gap between the energy ranges covered by EGRET and H.E.S.S. We explicitly demonstrate how our limits vary according to the assumed DM halo profile (our one source of uncertainty) and also compare our limit on the annihilation cross section to e^+e^- with corresponding bounds on the $\gamma\gamma$ and $\bar{\nu}\nu$ final states.

II. INTERNAL BREMSSTRAHLUNG

If DM annihilates to produce charged particles, the lowest order processes will always be subject to electromagnetic radiative corrections, resulting in the production of real photons. In particular, the annihilation $\chi\chi \to e^+e^-$ will be accompanied by the internal bremsstrahlung process $\chi\chi \to e^+e^-\gamma$. A photon may be emitted from either the final state e^+ or e^-, with a cross-section proportional to $\alpha \simeq 1/137$. See Refs. [36–38, 45] for a detailed discussion. To a good approximation, the differential cross section for $\chi\chi \to e^+e^-\gamma$ is

$$\frac{d\sigma_{\rm IB}}{dE} = \sigma_{\rm tot} \times \frac{\alpha}{E\pi}\left[\ln\left(\frac{s'}{m_e^2}\right) - 1\right]\left[1 + \left(\frac{s'}{s}\right)^2\right], \quad (1)$$

where E is the photon energy, $s = 4m_\chi^2$, $s' = 4m_\chi(m_\chi - E)$, and $\sigma_{\rm tot}$ is the tree-level cross section for $\chi\chi \to e^+e^-$. Note that $\sigma_{\rm tot}$ factors from the IB cross-section. This important feature implies that the IB spectrum is independent of the unknown physics which mediates the lowest order annihilation process. The photon spectrum per $\chi\chi \to e^+e^-$ annihilation is therefore given by

$$\frac{dN_\gamma}{dE} = \frac{1}{\sigma_{\rm tot}}\frac{d\sigma_{\rm IB}}{dE_\gamma}. \quad (2)$$

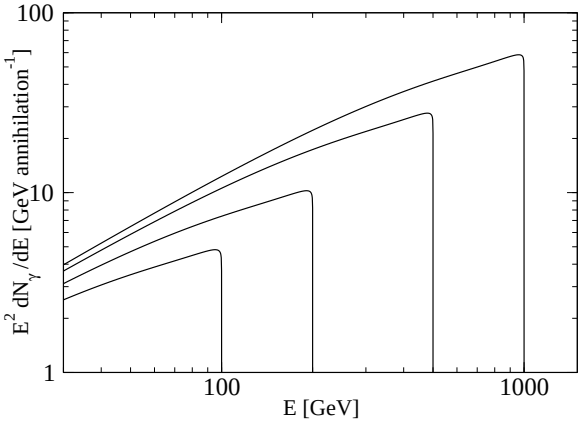

FIG. 1: Internal bremsstrahlung gamma-ray spectra per $\chi\chi \to e^+e^-$ annihilation, for $m_\chi = 100$, 200, 500, and 1000 GeV.

This spectrum is shown in Fig. 1 for various choices of the DM mass, where a sharp edge in the spectrum at $E = m_\chi$ is evident.

Note that we consider only radiation from the final state particles, and not from any internal propagators. In some supersymmetric scenarios in which s-channel annihilation to fermions is helicity suppressed, bremsstrahlung from internal propagators can be particularly important as it can circumvent this suppression [40–43]. We do not consider these model-dependent processes. Note, however, that the presence of such emission would only increase the gamma-ray flux we calculate, and hence strengthen the cross section limits derived.

III. ANNIHILATION IN DARK MATTER HALOS

The rate at which dark matter annihilates is proportional to the square of the dark matter number density, $n_\chi = \rho/m_\chi$. However, there are considerable uncertainties in the dark matter density profile of the galactic halo, particularly in the central region where the density, and hence the annihilation rate, is largest. To deal with these uncertainties, we make conservative assumptions about the DM density profile, and show how our results vary if less conservative assumptions were used.

A standard parameterization of a dark matter halo density profile is

$$\rho(r) = \frac{\rho_0}{(r/r_s)^\gamma\left[1 + (r/r_s)^\alpha\right]^{(\beta-\gamma)/\alpha}}. \quad (3)$$

The Kravtsov [46], Navarro-Frenk-White (NFW) [47] and Moore [48] profiles are defined by the values (α, β, γ) shown in Table I. The Milky Way values for r_s, the scale radius, and $\rho(R_{\rm sc})$, the DM matter density at the solar circle $R_{\rm sc} = 8.5$ kpc, are also given in Table I. The normalization ρ_0 is then fixed by $\rho(R_{\rm sc})$ and r_s. For large radii $r \gtrsim r_s$, all three profiles scale with radius as $1/r^3$

TABLE I: Values of the parameters (α, β, γ) which define the Kravtsov, NFW and Moore halo profiles. The values of the scale radius r_s in [kpc], and halo density normalization at the solar circle $\rho(R_{\rm sc})$ in [GeV cm^{-3}], are specific to the Milky Way.

	α	β	γ	r_s	$\rho(R_{\rm sc})$
Kravtsov	2	3	0.4	10	0.37
NFW	1	3	1	20	0.3
Moore	1.5	3	1.5	28	0.27

and are normalized such that they coincide closely. However, the profiles diverge for small radii, scaling as $1/r^{0.4}$, $1/r$ and $1/r^{1.5}$ for the Kravtsov, NFW and Moore profiles respectively. The steep Moore profile thus features a greatly enhanced density near the Galactic center, compared to the relatively flat Kravtsov profile; the NFW profile falls between the two.

Uncertainties in the density of the DM halo translate into uncertainties in the DM annihilation rate. A detailed discussion of the dependence of DM annihilation signals on the choice of density profile is given in Ref. [25]. While the uncertainties are mild for large angular regions of the galaxy, they scale several orders of magnitude for small angular scales close to the Galactic center. In order to place conservative upper limits on the DM annihilation cross section, we focus on the profile with the smallest dark matter density, namely the Kravtsov profile. For the NFW and Moore profiles, smaller values of $\langle \sigma_A v \rangle$ are needed to reproduce the same flux, and hence lead to stronger (less conservative) limits.

We now calculate the gamma-ray flux for annihilations in the galactic halo. For an observation direction at angle ψ with respect to the Galactic center, the integral of the square of the dark matter density along the line of sight is given by

$$\mathcal{J}(\psi) = {\rm J}_0 \int_0^{\ell_{max}} \rho^2 \left(\sqrt{R_{\rm sc}^2 - 2\ell R_{\rm sc} \cos\psi + \ell^2} \right) d\ell \,, \quad (4)$$

where ${\rm J}_0 = 1/[8.5\,{\rm kpc} \times (0.3\,{\rm GeV\,cm^{-3}})^2]$ is an arbitrary normalization constant used to make $\mathcal{J}(\psi)$ dimensionless, and which cancels in our final expression for the gamma-ray flux. We then define the average of $\mathcal{J}(\psi)$ over an observation region of solid angle $\Delta\Omega$ as

$$\mathcal{J}_{\Delta\Omega} = \frac{2\pi}{\Delta\Omega} \int_0^{\psi} \mathcal{J}(\psi) \sin\psi d\psi. \quad (5)$$

Values of $\mathcal{J}(\psi)$ and $\mathcal{J}_{\Delta\Omega}$ are given ψ in Fig. 2 of Ref. [25]. With these definitions, the gamma-ray flux per steradian due to DM annihilation in an observation region of angular size $\Delta\Omega$ is

$$\frac{d\Phi_\gamma}{dE} = \frac{\langle \sigma_A v \rangle}{2} \frac{\mathcal{J}_{\Delta\Omega}}{4\pi m_\chi^2 {\rm J}_0} \frac{dN_\gamma}{dE}, \quad (6)$$

where dN_γ/dE is the gamma-ray spectrum per annihilation. For the IB emission associated with annihilation to $e^\pm$, we must replace $\langle \sigma_A v \rangle$ with $\langle \sigma_A v \rangle_{e^+e^-} = \langle \sigma_A v \rangle \times {\rm Br}(e^+e^-)$, while dN_γ/dE is given by Eq. 2.

IV. ANALYSIS OF ANNIHILATION FLUX

A. Analysis technique

Our analysis technique is similar to that followed in Mack *et al.* [49]. We use galactic gamma-ray data from COMPTEL [50], EGRET [51] and H.E.S.S. [52], together spanning the broad energy range $10^{-3} - 10^4$ GeV. As there is a small gap between the energy ranges covered by EGRET and H.E.S.S., we use the observations of the M31 (Andromeda) galaxy made by CELESTE [53] to calculate constraints for this energy interval.

The galactic gamma-ray background measurements reported by COMPTEL, EGRET and H.E.S.S. are given in approximately log-spaced energy intervals, with energy bins of size ranging from $\Delta \log E \sim 0.2 - 0.6$. We calculate the IB gamma-ray flux for the observation regions viewed by these experiments, using the methods outlined above, and compare with the observational data. Upper limits on $\langle \sigma_A v \rangle_{e^+e^-}$ are determined by requiring that the IB flux due to DM annihilation be lower than 100% of the observed gamma-ray background flux in each of the experimental energy bins. Given that a large fraction of the observed gamma-ray background is likely to be astrophysical in origin, and not due to DM annihilation, taking the total background flux to be an upper limit on the DM annihilation signal is an extremely conservative approach.

For each energy bin, we take the DM mass to be equal to the upper energy limit of the bin, and integrate the IB flux over the width of the bin. Figure 2 shows the quantity

$$\int_{E_{\rm min}}^{m_\chi} \frac{dN_\gamma}{dE} dE = \frac{1}{\sigma_{\rm tot}} \int_{E_{\rm min}}^{m_\chi} \frac{d\sigma_{\rm IB}}{dE} dE, \quad (7)$$

which is the number of photons per annihilation as a function of bin size, for IB emission from $e^\pm$, and $m_\chi = 1000$ GeV. [Since m_χ enters Eq. 1 via a logarithm, variation with m_χ is only very mild.] This indicates how the size of the energy bins affects our results. For comparison, the number of photons per annihilation for the process $\chi\chi \to \gamma\gamma$ (for which $dN_\gamma/dE = 2\delta(m_\chi - E)$) is also shown. Note that the IB cross section is proportional to $1/E$, so for sufficiently low photon energy the IB probability becomes large and one must account for multiple photon emission. However, we are not working in this regime, and in fact obtain our limits using the flux near the endpoint of the spectrum. Despite the fact that the IB flux is small, we have enough hard gamma rays near the endpoint to result in strong bounds. For typical parameters, the IB flux per annihilation to $e^\pm$ is smaller

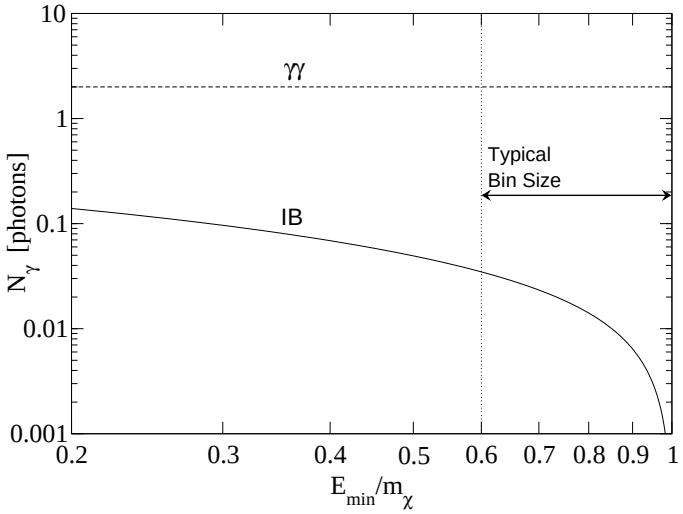

FIG. 2: Number of gamma rays per DM annihilation ($\int_{E_{\rm min}}^{m_\chi} dE\ dN_\gamma/dE$) as a function of the lower limit of integration, for IB emission from $\chi\chi \to e^+e^-$ (solid line). A typical bin size used in the analysis is shown. The DM mass used is 1000 GeV; variation with m_χ is very small. Shown for comparison is the number of photons per annihilation for the process $\chi\chi \to \gamma\gamma$ (dashed line) in which the photons are always at the endpoint.

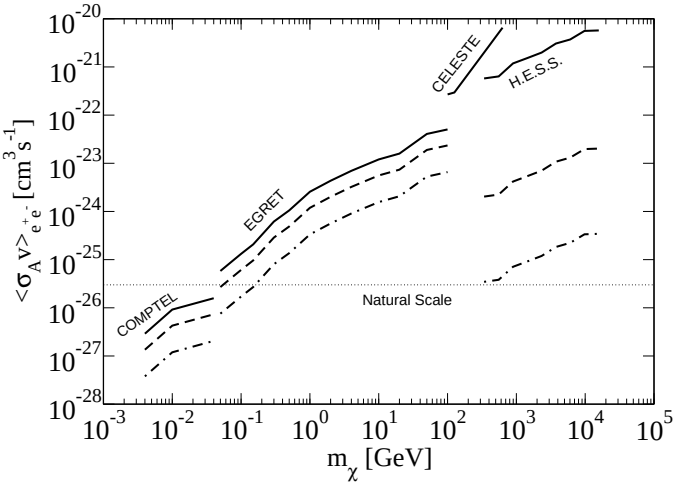

FIG. 3: Upper limit on $\langle\sigma v\rangle_{e^+e^-}$ as a function of DM mass for the Kravtsov (solid line), NFW (dashed line) and Moore (dotted-dashed line) profiles.

than the photon flux per annihilation for $\chi\chi \to \gamma\gamma$ by a factor of 10^2. This is expected, given that the IB cross section is suppressed by a factor of α with respect to the tree-level DM annihilation process.

B. Observational data

COMPTEL and EGRET are telescopes aboard the Compton Gamma-Ray Observatory. Refs. [54, 55] present flux data from these telescopes over an energy range of 1 MeV to 100 GeV between them, with a observation region of $-30^\circ < l < 30^\circ$ in Galactic longitude, and $-5^\circ < b < 5^\circ$ in Galactic latitude. We calculate $\mathcal{J}_{\Delta\Omega}$ as if the DM annihilation signal were from a circular region of $\psi = 30^\circ$. This is a conservative approach, as the average annihilation flux per steradian for the circular region is lower than for the rectangular region which was actually observed, and yields values of $\mathcal{J}_{\Delta\Omega} = (13, 28, 100)$ for the Kravtsov, NFW and Moore profiles respectively.

The H.E.S.S. observations reported in Ref. [56] cover the relatively small angular region $-0.8^\circ < l < 0.8^\circ$, $-0.3^\circ < b < 0.3^\circ$, in Galactic coordinates, over an energy range of 300 to 15 000 GeV. The data include a background subtraction which we must take into account when calculating $\mathcal{J}_{\Delta\Omega}$; see Mack *et al.* [49] for details. This leads to $\mathcal{J}_{\Delta\Omega} = (3, 850, 50\,000)$ for the Kravtsov, NFW and Moore profiles respectively.

CELESTE viewed the M31 galaxy with an observation region of angular radius 0.29°. No signal was seen, and a 2-σ upper limit on the flux of gamma rays from M31 between 50 and 700 GeV of around 10^{-10} photons cm^{-2} s^{-1} was reported [57] . We compare this flux with the IB signal calculated for an energy bin of size $10^{-0.4}m_\chi - m_\chi$. This is extremely conservative, as we are constraining the cross section by requiring that the annihilation flux in a small bin be less than or equal to the observed flux in a much larger bin. The DM density profile of M31 is less well constrained than that of the Milky Way. As in Ref. [49], we model the M31 halo using the Kravtsov profile for the Milky Way, which yields $\mathcal{J}_{\Delta\Omega} \times \Delta\Omega \simeq 2 \times 10^{-3}$.

V. DISCUSSION

In Fig. 3 we show the upper limits on $\langle\sigma_A v\rangle_{e^+e^-}$ as a function of DM mass, using the observational data described above. We give the Galactic genter results for the conservative Kravtsov profile, the more commonly adopted NFW profile, and the steep Moore profile. For the CELESTE observation of M31, differences between these profiles are expected to have a modest effect on the results, as a large portion of the galaxy is within the field of view; in Fig. 3 we show the CELESTE constraint using only the Kravtsov profile. As previously discussed, while the Kravtsov, NFW and Moore profiles diverge towards the center of the Galaxy, they are similar at large radii. As the EGRET and COMPTEL observations encompass relatively large angular scales, the density profile changes have a modest effect. On the other hand, the H.E.S.S. constraints correspond to a much smaller angular region toward the Galactic center, and vary by orders of magnitude depending on the profile adopted. (See Ref. [25] for a full discussion of the differences between the profiles for different angular regions.) To be conservative, we do not consider the possibility that DM annihilation

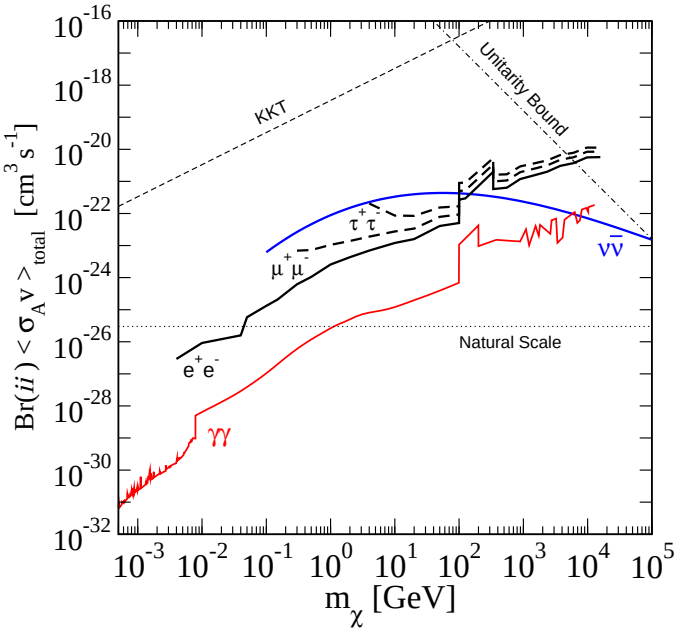

FIG. 4: Upper limits on the *partial* cross sections $Br(ii) \times \langle\sigma v\rangle_{total}$ for various final states $ii = e^+e^-$ (solid black line; labeled), $\mu^+\mu^-$ (thick dashed line; labeled), $\tau^+\tau^-$ (thick dashed line; labeled), $\gamma\gamma$ (red line; labeled), and $\bar{\nu}\nu$ (blue line; labeled), using the conservative Kravtsov profile. Each of these partial cross-section limits is independent, with no relationship assumed between the branching ratios to particular final states. Also shown are the KKT (thin dashed line) and unitarity (thin dotted-dashed line) limits on the *total* cross section described in the text, and the cross section for thermal relic DM (natural scale). The $\gamma\gamma$ and $\bar{\nu}\nu$ limits are taken from Ref. [49] and Ref. [25], respectively.

rates are enhanced due to substructure in the halo, e.g., Refs. [58–61], or mini-spikes around intermediate-mass black holes [62, 63]; such enhanced annihilation signals would result in stronger upper bounds on the cross section.

We can estimate the way that the cross-section bounds scale with the DM mass. The spectrum of the galactic gamma-ray background falls off with energy as $d\Phi/dE \sim E^{-\alpha}$ where, e.g., α is slightly larger than 2 in the EGRET and HESS energy ranges. The IB signal scales approximately as $d\Phi/dE \sim \langle\sigma_A v\rangle m_\chi^{-2} E^{-1}$ [where accounting the full energy dependence in Eq. 1 has only a small effect on this scaling]. Given this scaling with E, it is clear that the strongest constraints arise from the endpoint of the spectrum. In addition, small bin size is optimal for obtaining strong constraints. If we integrate the flux over an energy bin of width $x m_\chi$ to m_χ, the IB flux within the energy bin is proportional to $\langle\sigma_A v\rangle m_\chi^{-2}$ (ignoring logarithmic corrections) while the background flux is proportional to $m_\chi^{-\alpha+1}$ (for fixed x). The cross-section limits then scale with m_χ as $\langle\sigma_A v\rangle \sim m_\chi^{3-\alpha}$ and thus rise as m_χ if $\alpha \sim 2$.

In Fig. 4 we show the upper bounds on the annihilation cross sections into e^+e^-, $\mu^+\mu^-$, and $\tau^+\tau^-$, based upon the IB emission from each final state (all use the conservative Kravtsov profile). As the mass of the charged lepton increases, the rate of IB emission decreases and thus the upper bounds on the cross sections become weaker. However, as the IB spectrum depends only logarithmically on the charged lepton mass, this effect is mild, particularly for large DM mass. We have used Eq. 1 to calculate the IB flux over the entire mass range, and present limits which range from high m_χ down to just above threshold. We expect modifications to Eq. 1 in the limit that the charged leptons are nonrelativistic, but this will only affect a small mass range close to threshold. In the case of annihilation to $\tau^\pm$, we have not considered the gamma rays that arise from hadronic decay modes of the τ leptons (see, e.g., Ref. [38]) which form a broad spectrum centered on the pion mass.

Using Fig. 4, we may compare the limit on the annihilation cross section into e^+e^- with that for $\gamma\gamma$, taken from Ref. [49]. As anticipated, the bound on $\langle\sigma v\rangle_{e^+e^-}$ from IB is weaker than the bound on $\langle\sigma v\rangle_{\gamma\gamma}$ by a factor of $\sim 10^{-2} \sim \alpha$. This difference can be understood by comparing the number of hard gammas near the endpoint, $E_\gamma = m_\chi$. For annihilation to $\gamma\gamma$, there are always two monoenergetic gamma rays at the endpoint. The IB spectrum, integrated over a typical bin width (see Fig. 2) results in a flux that is smaller than this by only a factor of less than 100. That IB provides a limit this close to the ideal $\gamma\gamma$ channel illustrates the importance of the IB technique.

We stress that our IB limits apply to the *partial* DM annihilation cross sections, $\langle\sigma_A v\rangle_{l^+l^-}$, rather than the *total* annihilation cross section, $\langle\sigma_A v\rangle$. The two are related via $\langle\sigma_A v\rangle_{l^+l^-} = Br(l^+l^-)\langle\sigma_A v\rangle$. While the branching ratios are entirely dependent on the choice of DM model, there are many scenarios which feature large branching ratios for direct annihilation to leptons, such as Kaluza-Klein DM, or the recent models of Refs. [14–20]. Our constraints can be readily applied to any particular model, simply by dividing the $\langle\sigma_A v\rangle_{l^+l^-}$ bounds by the relevant branching ratios.

Also shown in Fig. 4 are a number of upper bounds on the *total* annihilation cross-section, based upon unitarity [22, 23] and the requirement that DM annihilation not significantly alter halo density profiles [Kaplinghat-Knox-Turner (KKT) [6]]. Note that the limit on annihilation to $\bar{\nu}\nu$ also defines a strong bound on the *total* DM annihilation cross section [24]. If we assume annihilation to only standard model final states, a conservative bound on the total cross section is obtained by assuming the branching ratio to neutrinos (the least detectable final state) is 100%. Any other assumption would lead to appreciable fluxes of gamma rays and hence be more strongly constrained. Dark matter annihilation into neutrinos was examined in Refs. [24] and [25]. The upper bound on $\langle\sigma_A v\rangle_{\bar{\nu}\nu}$ shown in Fig. 4 (taken from [25]) shows that the neutrino constraints are quite strong, particularly for large DM mass. (Reference [64] extended the

DM annihilation limits to lower masses, while Ref. [65] included substructure enhancement. Reference [66] derived analogous limits on the DM decay rate.) In fact, due to electroweak bremsstrahlung (radiation of W and Z bosons, rather than photons) neutrinos are also inevitably accompanied by photons [67–69]. However, this results in bounds that are comparable to, or weaker than, those obtained directly from neutrinos.

If DM annihilates to $e^{\pm}$, photons will be produced not only by IB, but also by energy loss processes including inverse Compton scattering and synchrotron radiation. In particular, radio wavelength signals produced via synchrotron emission have been the focus of much recent attention, e.g., [30–34]. However, the intensity of synchrotron radiation depends on a number of uncertain astrophysical parameters, such as magnetic field strength, radiation field intensities, and electron diffusion scales. By contrast, IB is free of these astrophysical uncertainties, and has a fixed spectrum and normalization. Another key difference is the energy of the photons. Synchrotron radiation produces generally low energy photons, while IB provides some hard gamma rays near the endpoint. Since the background flux falls off with energy, these hard gamma rays are extremely useful. The sharp edge in the IB spectrum at $E = m_{\chi}$ can be used to diagnose the DM mass; this is not possible with synchrotron radiation.

Nonetheless, it useful to take the synchrotron-based cross-section bounds as a reference point to compare with our IB-based bounds. Our conservative IB bound on $\langle \sigma_A v \rangle_{e^+e^-}$ is comparable to conservative bounds on $\langle \sigma_A v \rangle_{W^+W^-}$ obtained from synchrotron radiation. For example, Ref. [34] obtains $\langle \sigma_A v \rangle_{W^+W^-} \lesssim 4 \times 10^{-24}\mathrm{cm}^3\mathrm{s}^{-1}$ ($4 \times 10^{-23}\mathrm{cm}^3\mathrm{s}^{-1}$) at 100 GeV (1 TeV) assuming an NFW profile and conservative magnetic field choices (lower panel of Fig. 6 in Ref. [34]). This is to be compared with our IB result of $\langle \sigma_A v \rangle_{e^+e^-} \lesssim 2 \times 10^{-23}\mathrm{cm}^3\mathrm{s}^{-1}$ ($4 \times 10^{-24}\mathrm{cm}^3\mathrm{s}^{-1}$) at 100 GeV (1 TeV), again assuming an NFW profile. (The results of Ref. [34] are very similar to those of Ref. [32], though weaker than those of Ref. [31], in which less conservative assumptions were made.) Note that these synchrotron studies assume annihilation to W^+W^- (or $\bar{q}q$) which then decay to electrons, rather than direct annihilation to e^+e^-. Therefore, these electrons are not at the DM mass, and have instead a broad distribution of energies centered on the W mass. The synchrotron analyses in [31, 32, 34] thus serve only as an interesting reference point for our work, and not as a direct comparison.

References [14–20] have recently proposed models in which DM annihilates directly to charged leptons, with cross sections well above that expected for a thermal relic. This may account for anomalies in cosmic ray spectra from PAMELA, HEAT and ATIC, gamma-ray measurements from EGRET, and microwave signals from the Wilkinson Microwave Anisotropy Probe, all of which seem to require more electrons and positrons than can be explained otherwise. Our bounds on $\langle \sigma_A v \rangle_{l^+l^-}$ will directly constrain the allowed parameter space for these types of DM models.

We expect the sensitivity of the IB bounds to be improved by forthcoming data from the Fermi-GLAST experiment [70–72]. Improved point source subtraction enabling the diffuse background to be reduced, together with better energy and angular resolution and high statistics measurements, will enable stronger limits to be placed on all DM annihilation processes that produce gamma rays in the measured energy range.

VI. CONCLUSIONS

Dark matter annihilation into charged particles will necessarily be accompanied by gamma rays. Internal bremsstrahlung from final state charged particles can produce hard gamma rays, close to the endpoint defined by $E_{\gamma} = m_{\chi}$, with an approximately model-independent spectrum. Using galactic gamma-ray data, we have calculated upper limits on the dark matter annihilation cross section to e^+e^- and other charged leptons. We have made conservative assumptions about the astrophysical inputs, and demonstrated how our derived bounds would be strengthened if the galactic halo has a steeper density profile than assumed. The upper bound on the annihilation cross section into e^+e^- is weaker than that for the ideal $\gamma\gamma$ final state by only a factor of $\lesssim 10^2$. For a wide range of masses, our upper bound on $\langle \sigma_A v \rangle_{e^+e^-}$ is stronger than the bound on the total cross section defined by neutrinos, the least detectable final state. Compared with recent constraints on DM annihilation cross sections based upon synchrotron radiation, the internal bremsstrahlung constraints on $\langle \sigma_A v \rangle_{e^+e^-}$ are broadly comparable in strength. However, synchroton emission depends strongly on poorly known astrophysical inputs, such as galactic magnetic field strengths. In comparison, the normalization and spectrum of IB radiation is fixed, independent of any astrophysical inputs, and is thus an extremely clean technique.

Acknowledgments: We thank Gianfranco Bertone, Greg Mack, Stefano Profumo and Hasan Yuksel for helpful discussions, and John Beacom for detailed comments on the manuscript. NFB was supported by a University of Melbourne Early Career Research Grant, and TDJ by the Commonwealth of Australia.

[1] G. Jungman, M. Kamionkowski and K. Griest, Phys. Rept. **267**, 195 (1996). [arXiv:hep-ph/9506380].

[2] G. Bertone, D. Hooper and J. Silk, Phys. Rept. **405**, 279

(2005). [arXiv:hep-ph/0404175].
[3] L. Bergstrom, Rept. Prog. Phys. **63**, 793 (2000) [arXiv:hep-ph/0002126].
[4] S. Das and N. Weiner, [arXiv:astro-ph/0611353].
[5] M. Fairbairn and J. Zupan, arXiv:0810.4147 [hep-ph].
[6] M. Kaplinghat, L. Knox and M. S. Turner, Phys. Rev. Lett. **85**, 3335 (2000) [arXiv:astro-ph/0005210].
[7] J. Hisano, S. Matsumoto, M. M. Nojiri and O. Saito, Phys. Rev. D **71**, 063528 (2005) [arXiv:hep-ph/0412403].
[8] J. L. Feng and J. Kumar, arXiv:0803.4196 [hep-ph].
[9] J. March-Russell, S. M. West, D. Cumberbatch and D. Hooper, JHEP **0807**, 058 (2008) [arXiv:0801.3440 [hep-ph]].
[10] G. Servant and T. M. P. Tait, Nucl. Phys. B **650**, 391 (2003) [arXiv:hep-ph/0206071].
[11] H. C. Cheng, J. L. Feng and K. T. Matchev, Phys. Rev. Lett. **89**, 211301 (2002) [arXiv:hep-ph/0207125].
[12] D. Hooper and G. D. Kribs, Phys. Rev. D **70**, 115004 (2004) [arXiv:hep-ph/0406026].
[13] R. Harnik and G. D. Kribs, arXiv:0810.5557 [hep-ph].
[14] M. Cirelli, M. Kadastik, M. Raidal and A. Strumia, arXiv:0809.2409 [hep-ph].
[15] N. Arkani-Hamed, D. P. Finkbeiner, T. Slatyer and N. Weiner, arXiv:0810.0713 [hep-ph]. See also N. Arkani-Hamed and N. Weiner, arXiv:0810.0714 [hep-ph].
[16] M. Pospelov and A. Ritz, arXiv:0810.1502 [hep-ph].
[17] A. E. Nelson and C. Spitzer, arXiv:0810.5167 [hep-ph].
[18] I. Cholis, D. P. Finkbeiner, L. Goodenough and N. Weiner, arXiv:0810.5344 [astro-ph].
[19] Y. Bai and Z. Han, arXiv:0811.0387 [hep-ph].
[20] P. J. Fox and E. Poppitz, arXiv:0811.0399 [hep-ph].
[21] M. Kamionkowski and S. Profumo, arXiv:0810.3233 [astro-ph].
[22] K. Griest and M. Kamionkowski, Phys. Rev. Lett. **64**, 615 (1990).
[23] L. Hui, Phys. Rev. Lett. **86**, 3467 (2001) [arXiv:astro-ph/0102349].
[24] J. F. Beacom, N. F. Bell and G. D. Mack, Phys. Rev. Lett. **99**, 231301 (2007) [arXiv:astro-ph/0608090].
[25] H. Yuksel, S. Horiuchi, J. F. Beacom and S. Ando, Phys. Rev. D **76**, 123506 (2007) arXiv:0707.0196 [astro-ph].
[26] D. Fargion, R. Konoplich, M. Grossi and M. Khlopov, Astropart. Phys. **12**, 307 (2000) [arXiv:astro-ph/9809260].
[27] E. A. Baltz and L. Wai, Phys. Rev. D **70**, 023512 (2004) [arXiv:astro-ph/0403528].
[28] D. P. Finkbeiner, [arXiv:astro-ph/0409027].
[29] R. Aloisio, P. Blasi and A. V. Olinto, JCAP **0405**, 007 (2004) [arXiv:astro-ph/0402588].
[30] D. Hooper, D. P. Finkbeiner and G. Dobler, Phys. Rev. D **76**, 083012 (2007) [arXiv:0705.3655 [astro-ph]].
[31] D. Hooper, Phys. Rev. D **77**, 123523 (2008) [arXiv:0801.4378 [hep-ph]].
[32] E. Borriello, A. Cuoco and G. Miele, arXiv:0809.2990 [astro-ph].
[33] L. Zhang and G. Sigl, JCAP **0809**, 027 (2008) [arXiv:0807.3429 [astro-ph]].
[34] P. Grajek, G. Kane, D. J. Phalen, A. Pierce and S. Watson, arXiv:0807.1508 [hep-ph].
[35] T. E. Jeltema and S. Profumo, arXiv:0805.1054 [astro-ph].
[36] J. F. Beacom, N. F. Bell and G. Bertone, Phys. Rev. Lett. **94**, 171301 (2005) [arXiv:astro-ph/0409403].
[37] A. Birkedal, K. T. Matchev, M. Perelstein and A. Spray, arXiv:hep-ph/0507194.
[38] L. Bergstrom, T. Bringmann, M. Eriksson and M. Gustafsson, Phys. Rev. Lett. **94**, 131301 (2005). [arXiv:astro-ph/0410359].
[39] L. Bergstrom, T. Bringmann, M. Eriksson and M. Gustafsson, Phys. Rev. Lett. **95**, 241301 (2005) [arXiv:hep-ph/0507229].
[40] L. Bergstrom, Phys. Lett. B **225**, 372 (1989).
[41] E. A. Baltz and L. Bergstrom, Phys. Rev. D **67**, 043516 (2003) [arXiv:hep-ph/0211325].
[42] T. Bringmann, L. Bergstrom and J. Edsjo, JHEP **0801**, 049 (2008) [arXiv:0710.3169 [hep-ph]].
[43] L. Bergstrom, T. Bringmann and J. Edsjo, arXiv:0808.3725 [astro-ph].
[44] D. R. G. Schleicher, S. C. O. Glover, R. Banerjee and R. S. Klessen, arXiv:0809.1523 [astro-ph].
[45] M. E. Peskin and D. V. Schroeder, *An Introduction to Quantum Field Theory*, Ch. 6 (Addison-Wesley, Reading, 1995).
[46] A. V. Kravtsov, A. A. Klypin, J. S. Bullock and J. R. Primack, Astrophys. J. **502**, 48 (1998) [arXiv:astro-ph/9708176].
[47] J. F. Navarro, C. S. Frenk and S. D. M. White, Astrophys. J. **462**, 563 (1996) [arXiv:astro-ph/9508025].
[48] B. Moore, T. R. Quinn, F. Governato, J. Stadel and G. Lake, Mon. Not. Roy. Astron. Soc. **310**, 1147 (1999) [arXiv:astro-ph/9903164].
[49] G. D. Mack, T. D. Jacques, J. F. Beacom, N. F. Bell and H. Yuksel, Phys. Rev. D **78**, 063542 (2008) [arXiv:0803.0157 [astro-ph]].
[50] http://cossc.gsfc.nasa.gov/docs/cgro/cgro/comptel.html
[51] http://cossc.gsfc.nasa.gov/docs/cgro/cgro/egret.html
[52] http://www.mpi-hd.mpg.de/hfm/HESS/HESS.html
[53] http://doc.in2p3.fr/themis/CELESTE/
[54] A. W. Strong, H. Bloemen, R. Diehl, W. Hermsen and V. Schoenfelder, Astrophys. Lett. Commun. **39**, 209 (1999) [arXiv:astro-ph/9811211].
[55] A. W. Strong *et al.*, Astron. Astrophys. **444**, 495 (2005) [arXiv:astro-ph/0509290].
[56] F. Aharonian *et al.* [H.E.S.S. Collaboration], Nature **439**, 695 (2006) [arXiv:astro-ph/0603021].
[57] J. Lavalle *et al.*, Astron. Astrophys. **450**, 1 (2006) [arXiv:astro-ph/0601298].
[58] J. Diemand, M. Kuhlen and P. Madau, Astrophys. J. **657**, 262 (2007) [arXiv:astro-ph/0611370].
[59] L. E. Strigari, S. M. Koushiappas, J. S. Bullock, M. Kaplinghat, J. D. Simon, M. Geha and B. Willman, arXiv:0709.1510 [astro-ph].
[60] X. J. Bi, Nucl. Phys. B **741**, 83 (2006) [arXiv:astro-ph/0510714].
[61] D. Hooper and P. D. Serpico, JCAP **0706**, 013 (2007) [arXiv:astro-ph/0702328].
[62] G. Bertone, A. R. Zentner and J. Silk, Phys. Rev. D **72**, 103517 (2005) [arXiv:astro-ph/0509565].
[63] S. Horiuchi and S. Ando, Phys. Rev. D **74**, 103504 (2006) [arXiv:astro-ph/0607042].
[64] S. Palomares-Ruiz and S. Pascoli, Phys. Rev. D **77**, 025025 (2008) [arXiv:0710.5420 [astro-ph]].
[65] P. f. Yin, J. Liu, Q. Yuan, X. j. Bi and S. h. Zhu, arXiv:0806.3689 [astro-ph].
[66] S. Palomares-Ruiz, Phys. Lett. B **665**, 50 (2008) [arXiv:0712.1937 [astro-ph]].
[67] M. Kachelriess and P. D. Serpico, Phys. Rev. D **76**, 063516 (2007) [arXiv:0707.0209 [hep-ph]].
[68] J. B. Dent, R. J. Scherrer and T. J. Weiler,

arXiv:0806.0370 [astro-ph].
[69] N. F. Bell, J. B. Dent, T. D. Jacques and T. J. Weiler, Phys. Rev. D **78**, 083540 (2008) arXiv:0805.3423 [hep-ph].
[70] A. Morselli, Nucl. Phys. Proc. Suppl. **134**, 127 (2004) [AIP Conf. Proc. **745**, 422 (2005)].
[71] E. A. Baltz *et al.*, JCAP **0807**, 013 (2008) [arXiv:0806.2911 [astro-ph]].
[72] T. E. Jeltema and S. Profumo, arXiv:0808.2641 [astro-ph].